A Thesis Title

by

Allison Schneider

Submitted to the Dept. of Earth, Atmospheric and Planetary Sciences
in partial fulfillment of the requirements for the degree of

Bachelor of Science in Earth, Atmospheric and Planetary Sciences

at the

MASSACHUSETTS INSTITUTE OF TECHNOLOGY

September 2017

Author .....
Dept. of Earth, Atmospheric and Planetary Sciences
August 5, 2017

Certified by .....
Glenn R. Flierl
Professor of Oceanography
Thesis Supervisor

Accepted by .....
Richard P. Binzel
Chairman, Committee on Undergraduate Program

A Thesis Title

by

Allison Schneider

Submitted to the Dept. of Earth, Atmospheric and Planetary Sciences
on August 5, 2017, in partial fulfillment of the
requirements for the degree of
Bachelor of Science in Earth, Atmospheric and Planetary Sciences

Abstract

In this thesis, I designed and implemented a compiler which performs optimizations that reduce the number of low-level floating point operations necessary for a specific task; this involves the optimization of chains of floating point operations as well as the implementation of a "fixed" point data type that allows some floating point operations to simulated with integer arithmetic. The source language of the compiler is a subset of C, and the destination language is assembly language for a micro-floating point CPU. An instruction-level simulator of the CPU was written to allow testing of the code. A series of test pieces of codes was compiled, both with and without optimization, to determine how effective these optimizations were.

Thesis Supervisor: Glenn R. Flierl
Title: Professor of Oceanography

Acknowledgments

This is the acknowledgements section. You should replace this with your own acknowledgements.

Contents

List of Figures

List of Tables

1 Introduction

1.1 The Aerocene project

1.2 Acceleration from geopotential height

In a dynamic isobaric trajectory model, the acceleration of a parcel of air at a given pressure level can be determined from its velocity, latitude, and geopotential height. The geopotential height Z_g of a surface of pressure p above mean sea level is

$$Z_g(p) = R \int_p^{p_s} \frac{T}{g} \frac{dp}{p}, \tag{1.1}$$

where R is the gas constant, T is temperature, p_s is surface pressure, g is acceleration due to gravity at mean sea level, and $Z_g(p_s)$ is set to 0. In the troposphere, the difference between geopotential height and actual height is negligible [Marshall and Plumb, 2008].

The geopotential Φ is the potential energy of the Earth's gravitational field at a height h:

$$\Phi(h) = gZ_g(h). \tag{1.2}$$

The full equation for acceleration of an air parcel in the atmosphere is

$$\frac{D\vec{u}}{Dt} + \frac{1}{\rho}\nabla p + \nabla\Phi + f\hat{z} \times \vec{u} = \mathcal{F} \tag{1.3}$$

where $\vec{u}$ is the wind velocity vector, ρ is the density of air, f is the Coriolis parameter, and $\mathcal{F}$ is the force of friction per unit mass [Marshall and Plumb, 2008]. To implement this equation in the dynamic model, it must be written in terms of the zonal, meridional, and vertical wind components u, v and w. One assumption of the model is that friction is negligible at the studied pressure level, so $\mathcal{F}$ is taken to be zero.

$$\frac{Du}{Dt} + \frac{1}{\rho}\frac{\partial p}{\partial x} - fv = 0 \tag{1.4}$$

$$\frac{Dv}{Dt} + \frac{1}{\rho}\frac{\partial p}{\partial y} - fu = 0 \tag{1.5}$$

$$\frac{Dw}{Dt} + \frac{1}{\rho}\frac{\partial p}{\partial z} + g = 0. \tag{1.6}$$

The derivative of the geopotential is zero in the horizontal directions, and equal to g in the vertical following from Equation 1.2. Due to the isobaric assumption, the vertical velocity is zero, so Equation 1.6 becomes an expression of hydrostatic equilibrium:

$$\frac{1}{\rho}\frac{\partial p}{\partial z} + g = 0, \text{ or} \tag{1.7}$$

$$\frac{\partial p}{\partial z} = -\rho g. \tag{1.8}$$

Pressure can be defined as a function of the horizontal position and the geopotential height at that position at a given time:

$$p(x, y, Z_g(x, y, t), t) = p_0 \tag{1.9}$$

where p_0 is the studied pressure level. The partial derivatives of pressure with respect to x and y are

$$\frac{\partial p}{\partial x} + \frac{\partial p}{\partial Z_g}\frac{\partial Z_g}{\partial x} = 0 \tag{1.10}$$

$$\frac{\partial p}{\partial y} + \frac{\partial p}{\partial Z_g}\frac{\partial Z_g}{\partial y} = 0. \tag{1.11}$$

Using the hydrostatic relationship in Equation 1.8, these become

$$\frac{\partial p}{\partial x} = \rho g \frac{\partial Z_g}{\partial x} \tag{1.12}$$

$$\frac{\partial p}{\partial y} = \rho g \frac{\partial Z_g}{\partial y} \tag{1.13}$$

which can be substituted into Equations 1.4 and 1.5 to yield

$$\frac{Du}{Dv} = fv - g\frac{\partial Z_g}{\partial x} \tag{1.14}$$

$$\frac{Dv}{Dt} = -fu - f\frac{\partial Z_g}{\partial y}. \tag{1.15}$$

These equations are implemented in the dynamic model to determine the acceleration of air parcels over time.

2 Methods

Two trajectory calculation routines, a kinematic and a dynamic model, were written using Python's NumPy scientific computing package. Both routines numerically predict the trajectories of an ensemble of parcels by determining the velocities of parcels over time. The kinematic routine finds these velocities by interpolating between grids of wind speed data. The dynamic routine calculates velocities using advection equations relating the parcel acceleration and the geopotential height of a given pressure level.

2.1 Ten day dataset

Data from the Global Forecast System (GFS), a weather forecast model produced by the National Centers for Environmental Prediction (NCEP), was used for both models. The dataset chosen was a ten day forecast, starting at 12:00:00 on February 21st, 2017, with predictions at intervals of three hours. Each file in the dataset contains atmospheric predictions for the beginning of a three-hour interval. The values of atmospheric variables are predicted at each point on a latitude-longitude grid spanning the globe, with a spacing between gridpoints of 0.25 degree. Values are predicted for East-West and North-South wind speed components u and v, as well as the geopotential height Z_g of the 250 hectopascal (hPa) pressure level.

2.2 Linear interpolation

Both the kinematic and dynamic models require an interpolation scheme to produce values for atmospheric variables at positions between the gridded values provided by GFS. Linear interpolation is the standard choice for trajectory models [Bowman et al., 2013]. For both models, linear interpolation was used in three dimensions (latitude, longitude, and time). In the kinematic model, u and v components of wind speed were interpolated to the current positions of the air parcels, while in the dynamic model, geopotential height was interpolated.

2.3 Second-order integration scheme

The numerical scheme chosen was a second-order Runge-Kutta method which has a long track record in trajectory modeling [Petterssen, 1940]. The velocity at a given timestep is taken to be the average of the velocity at the initial position and the velocity at the first-guess position after one timestep.

The first guess position $\vec{P}'(t + \Delta t)$ is

$$\vec{P}'(t + \Delta t) = \vec{P}(t) + \vec{V}(\vec{P}, t)\Delta t \tag{2.1}$$

and the final position $\vec{P}(t + \Delta t)$ is

$$\vec{P}(t + \Delta t) = \vec{P}(t) + \frac{1}{2}\left[\vec{V}(\vec{P}, t) + \vec{V}(\vec{P}', t + \Delta t)\right]\Delta t \tag{2.2}$$

where $\vec{P}$ is a position vector with latitude and longitude components, and $\vec{V}$ a velocity vector with u and v wind speeds [Draxler and Hess, 1997]. This integration method is used by HYSPLIT and a number of other trajectory models, including FLEXPART, LAGRANTO, and STILT [Bowman et al., 2013, Stein et al., 2015] For trajectories calculated from interpolated gridded wind velocities, higher order integration schemes do not add precision [Draxler and Hess, 1997].

2.4 Constant timestep

For simplicity, both models employ a constant timestep. To save computation, HYSPLIT uses a dynamic timestep, varying from one minute to one hour, computed to satisfy

$$U_{max}[\text{grid-units min}^{-1}]\Delta t[\text{min}] < 0.75[\text{grid-units}] \tag{2.3}$$

[Draxler and Hess, 1997]. This ensures that the parcel does not blow past any grid squares during a single timestep, which maximizes the accuracy of the calculation. The value of the constant timestep for the experimental models was chosen so that Equation 2.3 is always satisfied. The process of choosing the timestep is detailed in Section 3.3.

2.5 Kinematic equations

At each timestep, after u and v speeds were interpolated and an average value found using the integration scheme, the kinematic model used two equations to solve for a parcel's displacement. The equations convert u and v provided by GFS in meters per second to time derivatives of latitude and longitude in radians. The r value of a parcel is taken to be the radius of the Earth R_E plus the parcel's geopotential height Z_g.

$$r = R_E + Z_g \tag{2.4}$$

$$\frac{d\varphi}{dt} = \frac{v}{r} \tag{2.5}$$

$$\frac{d\lambda}{dt} = \frac{u}{r\cos\varphi} \tag{2.6}$$

The initial conditions for these equations (latitude and longitude) are specified by

choosing the initial position of a parcel.

2.6 Dynamic equations

In the dynamic model, velocity at the next timestep was calculated using advection equations which incorporate the current geopotential height gradient and the previous timestep's u and v values. The Coriolis parameter f measures the effect of the Earth's rotation speed Ω at a given latitude φ. Standard acceleration due to gravity is g.

$$f = 2\Omega \sin \varphi \tag{2.7}$$

$$\frac{du}{dt} = fv - \frac{g}{r \cos \varphi} \frac{\partial Z_g}{\partial \lambda} \tag{2.8}$$

$$\frac{dv}{dt} = -fu - \frac{g}{r} \frac{\partial Z_g}{\partial \varphi} \tag{2.9}$$

Equations 2.8 and 2.9 are equations 1.14 and 1.15 transformed from Cartesian to geographic coordinates. After velocity at the next timestep is determined, the dynamic model also uses kinematic equations 2.5 and 2.6 to find the parcel position. This system of four differential equations requires four initial conditions: initial zonal and meridional velocities are needed in addition to initial latitude and longitude. Initial velocity components are set as the geostrophic wind at the initial position,

$$u_g = \frac{-g}{f} \frac{\partial Z_g}{\partial \varphi} \frac{1}{r} \tag{2.10}$$

$$v_g = \frac{g}{f} \frac{\partial Z_g}{\partial \lambda} \frac{1}{r \cos \varphi}. \tag{2.11}$$

2.7 The root-mean-square deviation measures parcel spread

For an ensemble of parcels, variance among trajectories over time was measured by calculating the mean trajectory: the path of an imaginary parcel whose position at each timestep is the average of the parcels' positions. At each timestep, the root-mean-square deviation (RMSD) is the square root of the average squared value of each particle's distance from the mean trajectory.

The mean trajectory was determined by finding the centroids of parcel positions at each timestep after converting trajectory latitudes and longitudes to three-dimensional Cartesian coordinates. NumPy's `arctan2(y,x)` is a two-argument arctangent function with a range of $(-\pi, \pi]$, N is the number of parcels, and n is the parcel index.

$$x_n = \cos\varphi_n \cos\lambda_n \qquad \bar{x} = \frac{1}{N}\sum_{n=1}^{N} x_n \tag{2.12}$$

$$y_n = \cos\varphi_n \sin\lambda_n \qquad \bar{y} = \frac{1}{N}\sum_{n=1}^{N} y_n \tag{2.13}$$

$$z_n = \sin\varphi_n \qquad \bar{z} = \frac{1}{N}\sum_{n=1}^{N} z_n \tag{2.14}$$

$$\bar{\lambda} = \arctan2\left(\bar{y}, \bar{x}\right) \tag{2.15}$$

$$\bar{\varphi} = \arctan2\left(\bar{z}, \sqrt{\bar{x}^2 + \bar{y}^2}\right) \tag{2.16}$$

The distance d between each parcel (with position φ_n, λ_n) and the mean parcel was calculated with the haversine formula

$$\Delta\varphi_n = |\varphi_n - \bar{\varphi}| \tag{2.17}$$

$$\Delta\lambda_n = |\lambda_n - \bar{\lambda}| \tag{2.18}$$

$$a_n = \sin^2\left(\frac{\Delta\varphi_n}{2}\right) + \cos\varphi_n \cos\bar{\varphi} \sin^2\left(\frac{\Delta\lambda_n}{2}\right) \tag{2.19}$$

$$c_n = 2 \cdot \arctan2\left(\sqrt{a_n}, \sqrt{1-a_n}\right) \tag{2.20}$$

$$d_n = R_E \cdot c_n \tag{2.21}$$

which is accurate and well-conditioned for small angles [Sinnott, 1984]. The RMSE at each timestep is calculated using the distance between each parcel and the mean parcel.

$$\mathrm{RMSE}\,(t) = \sqrt{\sum_{n=1}^{N} \frac{d_n(t)^2}{N}} \tag{2.22}$$

2.8 The absolute and relative horizontal transport deviation measure accuracy

Because the RMSE uses the mean trajectory as a reference value, it measures variance among trajectories of nearby parcels within a model. To compare trajectories between models, however, previous work has defined the absolute and relative horizontal transport deviation measures (AHTD and RHTD) [Stohl, 1998]. In this study, the AHTD is defined as

$$\mathrm{AHTD}\,(t) = \frac{1}{N}\sqrt{\sum_{n=1}^{N} d_n(t)^2} \tag{2.23}$$

This is similar to the RMSE, but the factor of $\frac{1}{N}$ has been moved outside the square root to agree with the standard definition [Kuo et al., 1985, Rolph and Draxler, 1990]. The values for d_n are calculated as in the RMSE, with the mean latitude $\bar{\varphi}$ and longitude $\bar{\lambda}$ in Equations 2.17 and 2.18 replaced by the latitude and longitude of a reference trajectory. The RHTD is the AHTD normalized by a length L_H.

$$\mathrm{RHTD}\,(t) = \frac{\mathrm{AHTD}\,(t)}{L_H} \tag{2.24}$$

In this study, L_H is defined as in Rolph and Draxler as the mean absolute horizontal travel distance of the reference trajectories.

$$L_H = \frac{1}{N}\sum_{n=1}^{N}\sqrt{\sum_{t=\Delta t}^{T} d_n(t)^2}. \tag{2.25}$$

This is a measure of the curved path length of the reference trajectory, not the distance between the starting and ending points as used by Kuo et al. [1985]. Here Δt is the timestep and T is the total trajectory time. Again d_n is calculated as in the RMSE, but with Equations 2.17 and 2.18 replaced by the difference between positions of a single parcel at two different timesteps:

$$\Delta\varphi_n = |\varphi_n(t) - \varphi_n(t - \Delta t)| \tag{2.26}$$

$$\Delta\lambda_n = |\lambda_n(t) - \lambda_n(t - \Delta t)|. \tag{2.27}$$

Although the "true" trajectories of parcels from the ten-day study period are unobservable, reference trajectories which approximate them can be calculated. Reference trajectories were obtained using NOAA's Real-time Environmental Applications and Display sYstem (READY), a tool which uses the HYSPLIT model to generate parcel trajectories [Rolph et al., 2017]. Analysis data from the Global Data Assimilation

System (GDAS), with a grid spacing of 0.5 degree and time resolution of three hours, was selected as the source of wind field information [NOAA, 2004]. Two kinds of reference trajectories were calculated with HYSPLIT: isobaric and three dimensional. Isobaric trajectories use the same vertical transport assumption as the experimental models. Three-dimensional trajectories model the vertical as well as the horizontal wind. Fully three-dimensional trajectories and analysis data are more accurate than isobaric trajectories and forecast data, so the reference trajectories will be closer to the "true" parcel trajectories than those calculated by the kinematic and dynamic models. [Stohl, 1998]. Comparing the HYSPLIT isobaric reference trajectories to the HYSPLIT 3D trajectories measures the contribution of the isobaric assumption alone to trajectory error.

3 Tuning the models

3.1 Inertial circles in the dynamic model

When the dynamic model was tested, some trajectories traced out large spirals, behavior uncharacteristic of atmospheric flow. Figure 3-1 shows an example of one such trajectory. The parcel's spiral is a result of the Coriolis force term in the dynamic equations. In the Northern Hemisphere, the direction of the Coriolis force is to the right of a parcel's motion. [[[Why are inertial circles observed in the ocean and not the atmosphere? What metric predicts this? Ekman number?]]]

The period T and radius R of an inertial circle are

$$T = \frac{2\pi}{f} \tag{3.1}$$

$$R = \frac{v}{f} \tag{3.2}$$

where f is the Coriolis parameter.

[[[To do: show that period and radius of this trajectory are what you'd expect for an inertial circle.]]]

3.2 Adding friction to the dynamic model

Previous studies have observed inertial circles in trajectories calculated with dynamic models which become particularly apparent for trajectories longer than 24 hours.

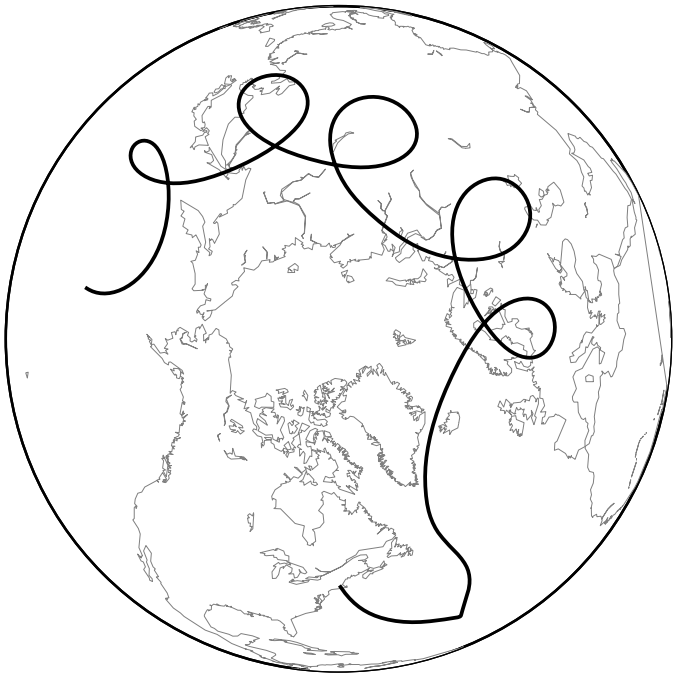

Figure 3-1: A parcel launched from 41.75°N, 71.25°W. Five inertial circles are visible in the latter part of the trajectory.

Figure 3-2: *Left*: Twenty five trajectories calculated with the frictionless dynamic model. Parcels were launched in an evenly-spaced 5x5 grid with its lower-left corner at 41°N, 72°W and upper-right corner at 42°N, 71°W. The large spirals are implausible for jet stream flow and reflect a problem with the model. *Right*: The same parcels with trajectories calculated by the dynamic model with friction. A few parcels still exhibit unrealistic spirals, but in general, trajectories are more plausible.

[Stohl and Seibert, 1998] One approach to mitigating oscillations, used by Stohl and Seibert, is to take a weighted average of the wind speeds from the dynamic model and interpolated speeds from a kinematic model at each timestep. Another approach is to change the frictionless assumption of the dynamical model. The force of friction has the effect of damping oscillations due to inertial motion. Using the definition of geostrophic wind in Equations 2.10 and 2.11, Equations 2.8 and 2.9 with an added friction term become

$$\frac{du}{dt} = f(v - v_g) - r_f(u - u_g) \tag{3.3}$$

$$\frac{dv}{dt} = -f(u - u_g) - r_f(v - v_g). \tag{3.4}$$

The damping term r_f is analogous to the Coriolis parameter: it has units of second^{-1} and is a measure of the force of friction. The value chosen for r_f was 10^{-6} seconds^{-1}, or 10 days^{-1}, a rough order of magnitude guess based on the experimental trajectory lengths.

Adding friction terms to the dynamic model reduces inertial oscillations significantly, as demonstrated in Figure 3-2. The terms were added to the dynamic model used in the Results section.

3.3 Choosing a timestep

The threshold that HYSPLIT uses to calculate its dynamic timestep, Equation 2.3, can also be expressed as the difference between a threshold velocity and trajectory velocity. If the trajectory velocity is greater than the threshold velocity at any time, the timestep is too short. Therefore, the conditions for velocity components in the u and v directions are

$$\frac{0.75sm\cos\varphi}{\Delta t} - u(t)_{max} < 0 \tag{3.5}$$

$$\frac{0.75sm}{\Delta t} - v(t)_{max} < 0 \tag{3.6}$$

The maximum fraction of a grid square a parcel should travel in one timestep is 0.75. There spatial resolution, s, is the number of degrees per grid square: for this dataset, 0.25. The conversion factor m between degrees latitude and distance is 111,320 meters.

These differences were plotted along an ensemble of test trajectories: 25 parcels launched in a 5x5 grid around Boston, Massachusetts, between 41°N, 72°W and 42°N, 71°W on February 21st, 2017 at 12:00 UTC. These trajectories were calculated with the kinematic model and the dynamic model with added friction. For both calculation schemes, the parcels can be observed to flow into the subtropical jet, which contains some of the highest windspeeds at the studied pressure level. As a result, a timestep tuned to these parcels should be appropriate for most trajectories. The first timestep tested was three minutes, as shown in Figure 3-3. Zonal speeds for dynamic trajectories surpass the threshold a number of times, indicating that a timestep of three minutes is too long.

The same trajectories were calculated using a shorter timestep of one minute and thirty seconds, as shown in Figure 3-4. Here, velocities are below the threshold at all times along the trajectory. With the exception of two dynamic trajectories, the threshold velocity is at least 50 meters per second greater than the observed velocity. Since one minute and thirty seconds was a sufficiently short timestep for this dataset, it was chosen as the timestep for all other model runs.

3.4 Initializing velocity for the dynamic model

The proposed method for determining initial trajectory velocity in the dynamic model was using the geostrophic wind, as expressed in Equations 2.10 and 2.11. The

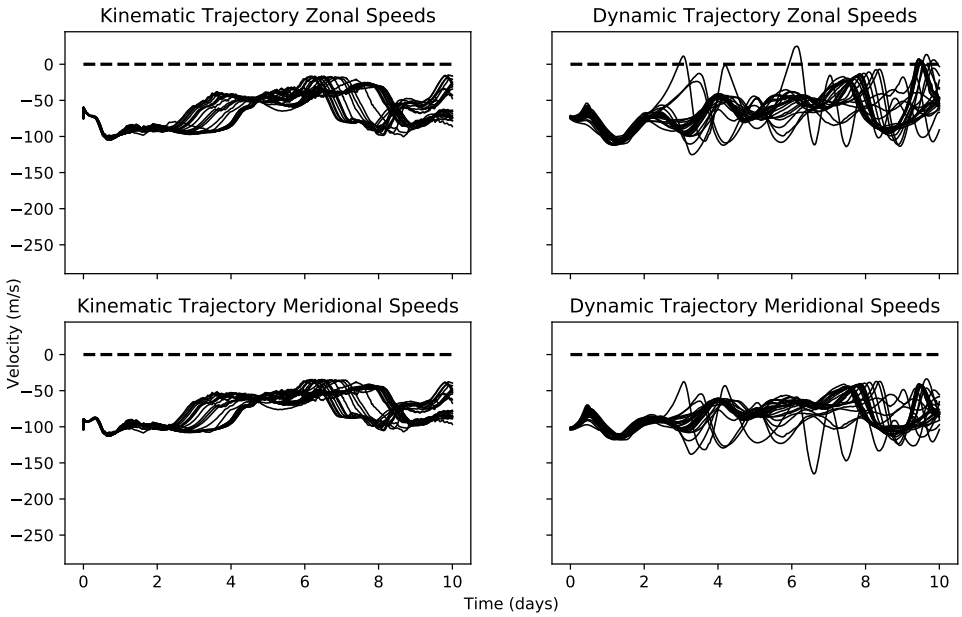

Figure 3-3: For a timestep of 3 minutes, trajectory speed is compared to threshold speed. Solid lines represent the threshold speed minus the trajectory speed for a timestep of 3 minutes. The dashed line at a velocity of zero represents the speed threshold. Note in the upper-right hand plot that the zonal speeds for some trajectories surpass the threshold.

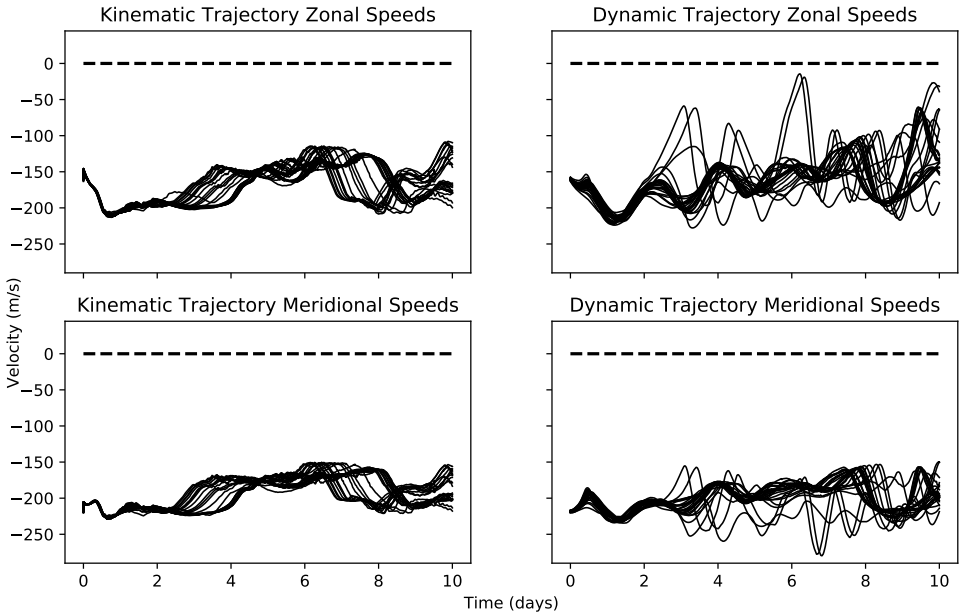

Figure 3-4: For a timestep of 1 minute and 30 seconds, trajectory speed is compared to threshold speed. For this choice of timestep, all parcel velocities are below the threshold.

geostrophic wind is the theoretical wind calculating using the assumption that the Coriolis force balances the pressure gradient force.

This method is attractive for two reasons. For one, it does not require additional data to be added to the dynamic model. Geostrophic wind is calculated using the same grid of geopotential height gradients used for the advection equations 2.8 and 2.9. For another, initializing wind speed with geostrophic wind may reduce the inertial circle behavior observed in the dynamic model, which results from wind speeds deviating from the geostrophic approximation.

However, the geostrophic approximation of wind speed breaks down near the equator. Figure 3-5 shows the ratio of zonally averaged geostrophic wind speeds to zonally averaged gridded wind speeds in the first file of the study period. For most latitudes, the ratio is close to 1, which indicates that the geostrophic wind is a reasonable assumption. Between 20S and 20N, the geostrophic wind becomes much greater than the observed wind. As the latitude goes to zero, the Coriolis parameter f in Equations 2.8 and 2.9 blows up, and the resulting geostrophic wind becomes

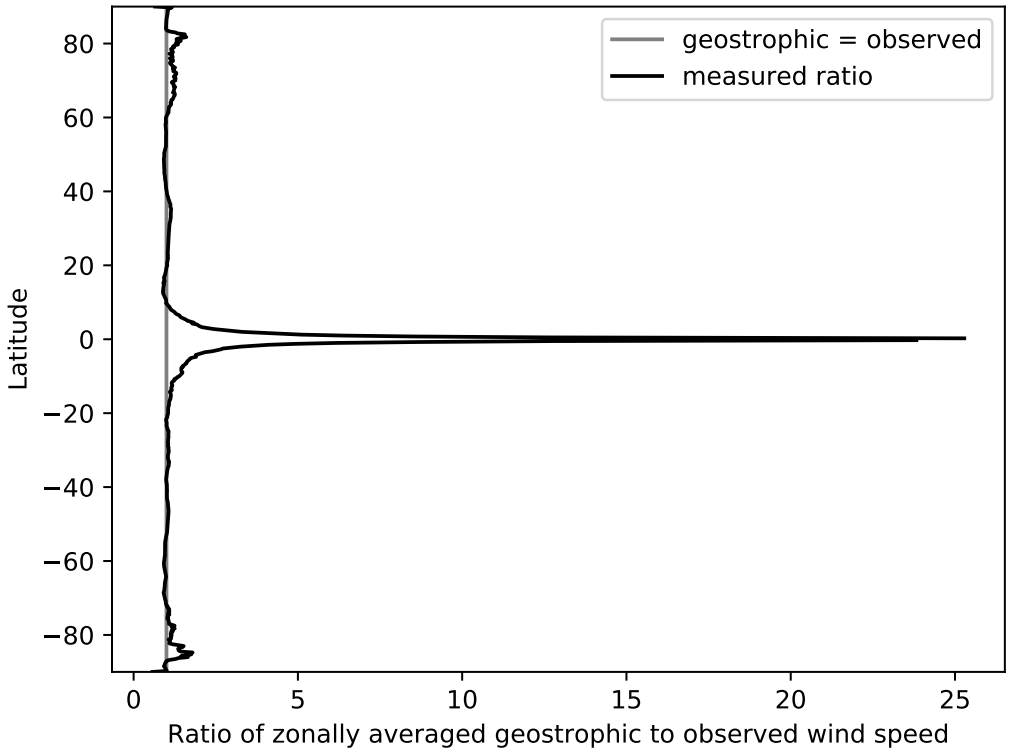

Figure 3-5: The ratio of zonally averaged geostrophic wind speed to zonally averaged geostrophic wind speed as a function of latitude. Near the Equator, the ratio increases sharply, indicating that the geostrophic approximation is invalid there.

unphysical.

Since the dynamic model is intended to produce accurate trajectories for the whole Earth, the geostrophic wind cannot be used. Instead, velocities were initialized with the gridded wind values at the trajectory start locations. This may increase inertial circle prevalence, but the initial deviation from the geostrophic wind is damped by the dynamic model's friction term. It also requires that wind speed data is available at every grid point in addition to geopotential height data, but this is likely to be the case when data from a forecast model like GFS is used.

4 Results

4.1 Measures of transport error

[[[The area containing the ensemble of parcels should grow as $t^{1/2}$, so should the RMSE as well? The errors of neighboring points are highly correlated, so the RMSE shows the general $t^{1/2}$ trend, but there's a lot of noise based on idiosyncrasies of the flow in that region. Maybe plot average RSME of all experiment locations over time?

The AHTD and RMSE are analogous to standard deviation. We discussed finding error bars on the AHTD and RHTD values by calculating them for ensembles started nearby: shifted a degree in every direction, for example. I could find the mean and standard deviation of AHTD and RHTD for the 3x3 grid of ensembles created by shifting the starting ensemble north/south/east/west. Are the shifted ensembles still in the same flow regime? How generalizable are error bars on AHTD and RHTD to the whole model, then?

Perhaps AHTD and RHTD are better measures for a larger grid, to get a measure of trajectory error for the whole model. In that case, instead of the 3x3 grid of trajectory ensembles, I could try a mesh of trajectory starting points over the whole globe. 6 degree spacing or so. The AHTD and RHTD would be a "whole model" reference, to which the AHTD and RHTD for more specific ensemble launch locations (like Boston) could be compared.]]]

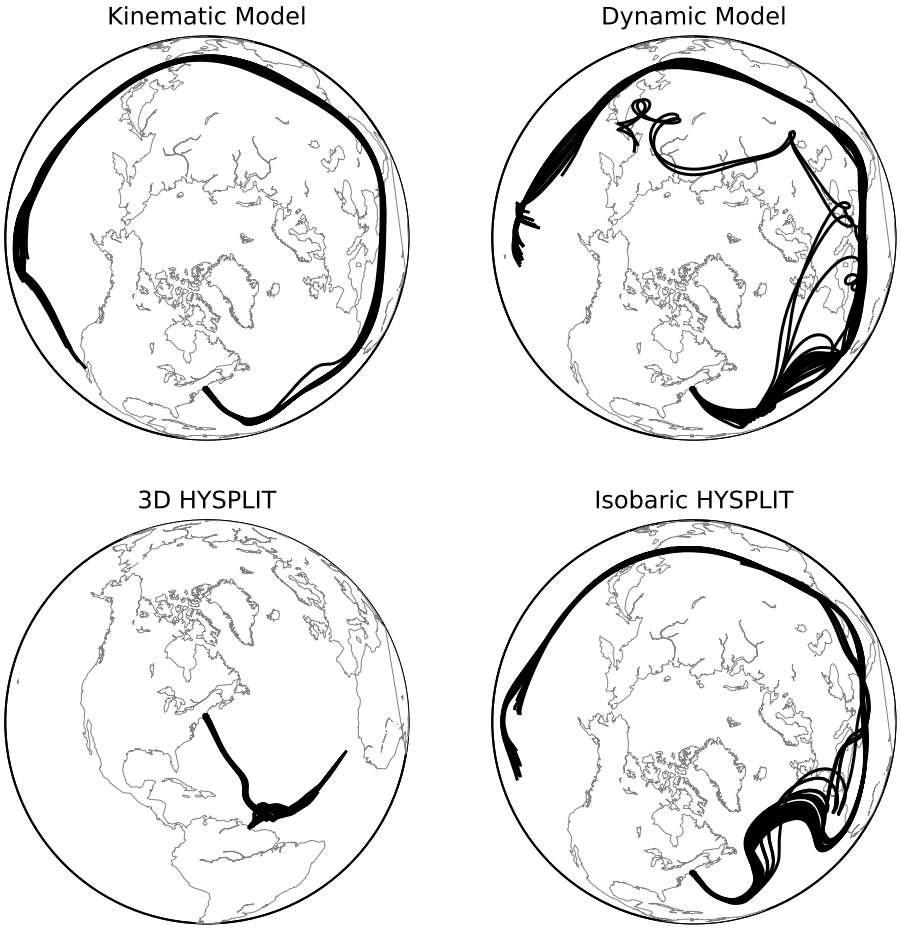

Figure 4-1: Trajectories for both models with reference trajectories for parcels launched from the 5x5 grid between 41°N, 72°W and 42°N, 71°W.

Table 4.1: Measures of transport error after 213 hours.

			Location	
Statistic	Model	Reference	Boston	Barau
RMSE	kinematic	mean trajectory	1,444 km	1,342 km
	dynamic	mean trajectory	2,800 km	5,607 km
	HYSPLIT 3D	mean trajectory	5,630 km	2,270 km
	HYSPLIT isobaric	mean trajectory	4,740 km	1,260 km
AHTD	kinematic	HYSPLIT 3D	2,160 km	1,130 km
	dynamic	HYSPLIT 3D	1,940 km	1,630 km
	kinematic	HYSPLIT isobaric	1,270 km	1,300 km
	dynamic	HYSPLIT isobaric	1,200 km	1,730 km
	HYSPLIT isobaric	HYSPLIT 3D	1,930 km	588 km
RHTD	kinematic	HYSPLIT 3D	0.48	0.92
	dynamic	HYSPLIT 3D	0.43	1.30
	kinematic	HYSPLIT isobaric	0.23	1.20
	dynamic	HYSPLIT isobaric	0.22	1.60
	HYSPLIT isobaric	HYSPLIT 3D	0.012	0.019

Bibliography

[Bowman et al., 2013] Bowman, K., Lin, J. C., Stohl, A., Draxler, R., and Konopka, P. (2013). Input data requirements for Lagrangian trajectory models. *Bulletin of the American Meteorological Society*, 94(7):1051–1058.

[Draxler and Hess, 1997] Draxler, R. R. and Hess, G. D. (1997). Description of the HYSPLIT_4 modeling system. Technical report, NOAA Air Resources Laboratory, Silver Spring, MD.

[Kuo et al., 1985] Kuo, Y., Skumanich, M., Haagenson, P. L., and Chang, J. S. (1985). The Accuracy of Trajectory Models as Revealed by the Observing System Simulation Experiments. *Monthly Weather Review*, 113:1852–1867.

[Marshall and Plumb, 2008] Marshall, J. and Plumb, R. A. (2008). *Atmosphere, Ocean, and Climate Dynamics: An Introductory Text*, volume 93 of *International Geophysics Series*. Elsevier Academic Press.

[NOAA, 2004] NOAA (2004). Global Data Assimilation System (GDAS1) Archive Information. Technical report, NOAA-Air Resources Laboratory, Silver Spring, MD.

[Petterssen, 1940] Petterssen, S. (1940). *Weather Analysis and Forecasting*. McGraw-Hill Book Company, New York.

[Rolph and Draxler, 1990] Rolph, G. D. and Draxler, R. R. (1990). Sensitivity of Three-Dimensional Trajectories to the Spatial and Temporal Densities of the Wind Field. *Journal of Applied Meteorology*, 29:1043–1054.

[Rolph et al., 2017] Rolph, G. D., Stein, A. F., and Stunder, B. J. B. (2017). Real-time Environmental Applications and Display sYstem: READY. *Environmental Modelling & Software*, 95:210–228.

[Sinnott, 1984] Sinnott, R. W. (1984). Virtues of the Haversine. *Sky & Telescope*, 68(2):159.

[Stein et al., 2015] Stein, A. F., Draxler, R. R., Rolph, G. D., Stunder, B. J. B., Cohen, M. D., and Ngan, F. (2015). NOAA's HYSPLIT Atmospheric Transport and Dispersion Modeling System. *Bulletin of the American Meteorological Society*, 96:2059–2077.

[Stohl, 1998] Stohl, A. (1998). Computation, accuracy and applications of trajectories—a review and bibliography. *Atmospheric Environment*, 32(6):947–966.

[Stohl and Seibert, 1998] Stohl, A. and Seibert, P. (1998). Accuracy of trajectories as determined from the conservation of meteorological tracers. *Quarterly Journal of the Royal Meteorological Society*, 124:1465–1484.